# DESIGN OF MICRO FLOW SENSOR FOR SLOWLY MOVING BIOLOGICAL FLUIDS IN SMART CATHETERS

[1]ENIKO T. ENIKOV, [2]GERGO EDES, [3]REIN ANTON, [4]MICHAEL LEMOLE

University of Arizona
E-mail: enikov@email.arizona.edu

**Abstract** - his paper reports on a the design and testing of a micro-flow sensor intended for use in implantable ventricular-peritoneal shunts. The detection of flow is based on flexible ferromagnetic flaps whose deflection is detected by ultra-sensitive magnetic (MTJ) sensors. Initial tests of the sensor unveiled significant low-frequency noise (drift) limiting the sensitivity to 1.4 mL/hr. The present study identifies thermal noise as the main source of low-frequency drift. Using thermal compensation it is demonstrated that the drift can be reduced below 3.2 mL per 24-hr. Further improvements are due to use of multiple (four) in-line transducers leading to a sensitivity increase of 7.2 fold.

**Index Terms** - VP shunt; Flow sensor; Thermal noise; MEMS; MTJ sensor

## I. INTRODUCTION

Magnetic tunneling junction (MTJ) sensors are finding ever more diverse applications. One such area is the detection of slow-moving fluids in medical catheters [9]. Unfortunately, MTJ sensors are prone to thermal noise, which could present itself as a low-frequency drift. Drainage of cerebral spinal fluid is important in the treatment of hydrocephalus, which has an incidence rate of 5.5 per 100,000 [1]. In a typical application, the drainage shunts are implanted sub-cutaneously as illustrated in Fig.1. A common failure mode of implanted cerebrospinal fluid shunts is occlusion or fouling of the catheter which occurs in 40 % of the implanted shunts during the first year, in 50 % by the end of the first two years and as high as 80 % during the lifetime of the implant [2,3,4]. Today around 10 % of deaths related to hydrocephalus are caused by shunt failure, despite significant advances in shunt design [5]. The high failure rate leads to over 27,000 surgeries every year that are aimed to repair or diagnose a failing shunt [6].

The need for continuous monitoring of the shunt flow has long been recognized, leading to the first published account of a telemetric, in-line, implanted device due to Atkinson et al. in 1967 [7]. Instead of flow measurements, the device measured changes in intra-cranial pressure (ICP). More recent efforts in the early 1980-ies were aimed at producing a batteryless prototype [8] however without demonstration of a functioning unit. More recent efforts to develop a working flowsensor have been reported by Enikov et al. utilizing MTJ sensors with micro-machined transduction element [9].

The latter publication has shown the proof of principle of flow sensors using a MEMS microfabricated ferromagnetic structures [9] however it also identified challenges represented by low-frequency noise. In this paper we present a systematic design and optimization of the original concept leading to an increase of signal to noise ration and elimination of the flow-frequency drift. The structural stability of the device was also studied in order to estimate its useful life.

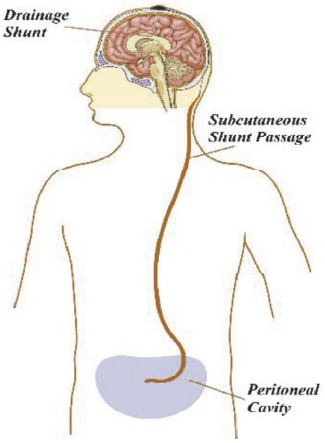


**Fig. 1 Placement of VP shunt**

## II. DETECTION MODE

The transducer is based on detecting Stokes drag through placing a flexible thin flap inside the fluid stream (see Fig. 2). The resulting drag causes the flap to bend in the direction of the flow, thus distorting the magnetic field created by a permanent magnet placed under the ferromagnetic transducer. The change in magnetic field is then detected by a magnetic (MTJ) sensor mounted near the movable transducer.

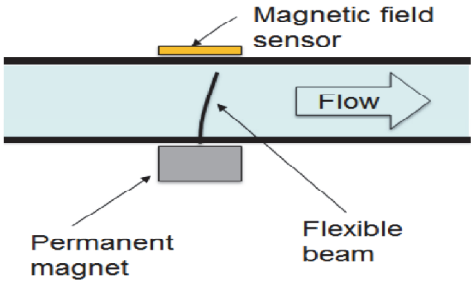


**Fig. 2 Flow detection principle.**

The particular type of magnetic sensor used in this work contains magnetic tunnel junctions (MTJ) between two layers of electrodes, separated by an ultra-thin insulator. The insulating layer is sufficiently thin to allow electrons to tunnel through it under a bias voltage. The tunneling current is based on the magnetization of the two metallic layers and hence modulated by the external magnetic field. If the direction of magnetization of one layer is parallel to the other the electrons have a higher probablility of tunneling through the barrier thus increasing the tunneling current. Conversely, if the two layers have opposite magnetization, the tunneling current is reduced. Therefore the changes in flow rate are detected by measuring the resistance changes of these MTJ sensors. Figure 3 shows the measurement circuit used for detecting resistance change in the MTJ sensor. In addition to the two-stage amplification, the circuit provides low-pass filtering with a cutoff frequency of 6 Hz.

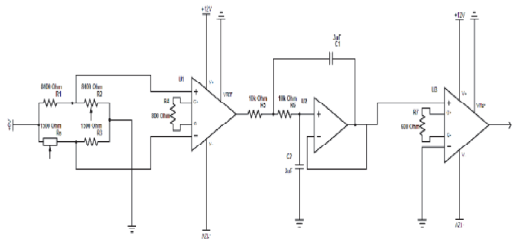

**Fig. 3 Sensor Signal Conditioning Circuit**

## III. SENSOR DESIGN IMPROVEMENTS

Under normal physiological conditions, the central nervous system discharges 450-550 ml of CSF per day. This is equivalent of 20 ml/hr. Due to cardiovascular pulsations, the flow is likely pulsatile with an estimated rage of 1-100 ml/hr. Therefore, the desired resolution of the sensor is approximately 1 ml/hr. In a previous study, we have presented a working prototype with a sensitivity of 25 mV/ml/h, which is easily detectable in the absence of noise. However, low-frequency drift necessitated a re-design aimed at increasing the signal to noise ration. The following sections describe these improvements.

### A. Mechanical Design

The first prototype used a relatively large flow channel (2 mm x 4 mm ) in order to facilitate assembly as shown in Fig.4 (left). The present version utilizes a smaller channel, thus maximizing the local flow rate and associated drag on the transducer. Concurrently the smaller transducer had to be more flexible, which led to geometric modification of the shape of the transducer shown in Fig.4 (center).

The increased flexibility of the new sensor was achieved by reduction of the width of the hinges, increasing their lenght, while the gap between the hinges was reduced. Having excessively long legs is also undesirable, as it leads to bending in the opposite direction. Therefore a finite element analysis was used to optimize the geometry. The resulting leg length vs deflection is shown in Figure 5.

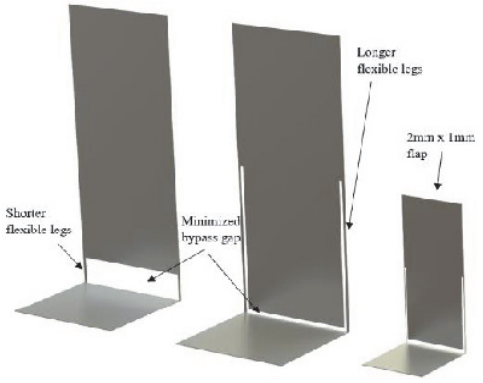


**Fig. 4 New vs Old Transducer Design**

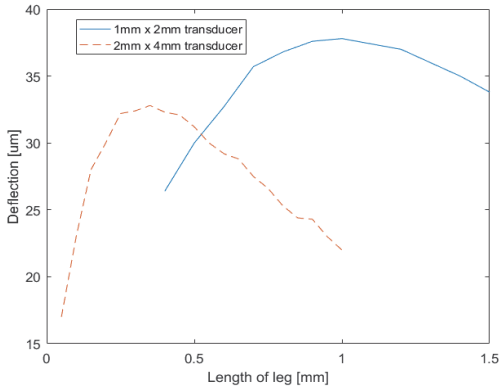


**Fig. 5 Optimization of leg height**

This design proved to be challenging to manufacture and implement as the large aspect ratio of the legs caused it to be very fragile during the assembly process and even after successful assembly the pulling force of the permanent magnet caused buckling to occur in the legs, thus hindering the mobility of the transducer. The cause of the buckling is shown in Fig.6. The resulting test data with the new design is shown in Fig.7. The buckling of the legs caused the bottom of the transducer to latch against the bonding pad, limiting flexibility at low flow rates.

At higher flow rates, the fluid pressure was large enough to release the top part of the transducer from the bonding pad, which resulted in a sudden voltage change in the signal output.

In the figure we can see the transducer measuring flow rates of around 3000 ml/h, with limited sensitivity below about 1.5V.

In order to reduce the aspect ratio of the device and improve reliability and implantability while improving on the sensitivity of the original design, the dimensions of the transducer were reduced to 1 mm x 2 mm. The miniaturized design is shown in Fig.4.

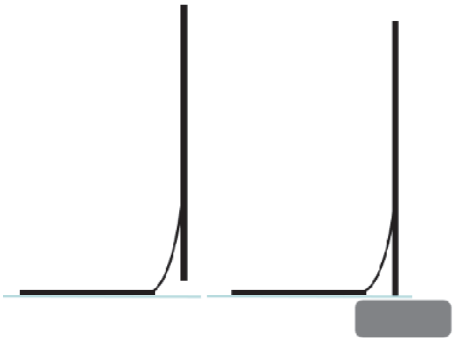

**Fig. 6Buckling of the transducer in the presence of a magnet**

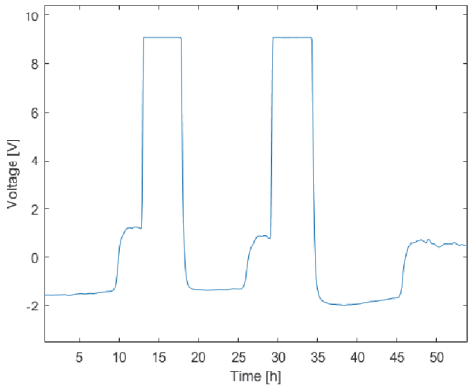


**Fig. 7Output from Latching Transducer**

The exact dimensions of the new transducer were obtained using a commercial numerical analysis tool (CFX, Ansys Inc.). The FEA model contained 329,420 tetrahedral elements with zero-slip boundary conditions applied on the side walls of the channel, while the nodes at the outlet were subjected to zero relative pressure. A preset mass flow rate was applied to the nodes corresponding to the channel inlet. Figure8 shows a comparison between the sensitivities of the original and the new design for flow rates in the range from 10 to 100 ml/h. When configured into a Wheatstone bridge, i.e. four sensors are used in each of the four branches of the bridge, the sensitivity of the new configuration increased from 25 mV/ml/h to 43 mV/ml/h, representing a 1.7 fold improvement.

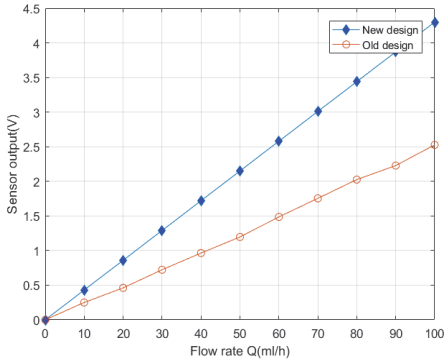


**Fig. 8 Simulated voltage output comparing the old and new transducer designs**

## B. Low Frequency Noise Analysis

Measurements taking from the old sensor over 24 hours showed a significant low-frequency drift [9]. Possible causes of the drift could be a mismatch between the temperature coefficient of resistance (TCR) of the resistors in the Wheatstone bridge. Another source of thermal noise are the two amplifiers producing a combined gain of 3300. Thus the investigation focused on correlating temperature fluctuations of the environment around the sensor with its output. To this end a temperature sensor was attached to the MTJ sensors and recordings were made over a period of 24 hours. Data displayed in figure 9 revealed a strong correlation between the temperature readings and the sensor output. A correlation plot is shown in figure 10 demonstrating a temperature sensitivity of 3.9 V/ ˚C .

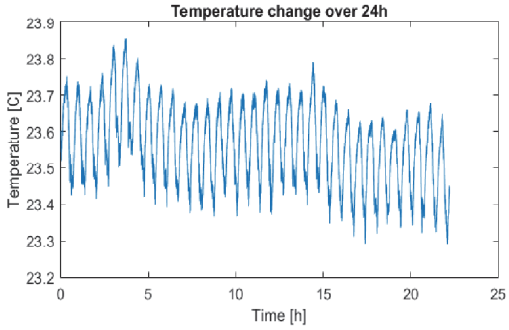


**Fig. 9Data output from magnetic and temperature sensors**

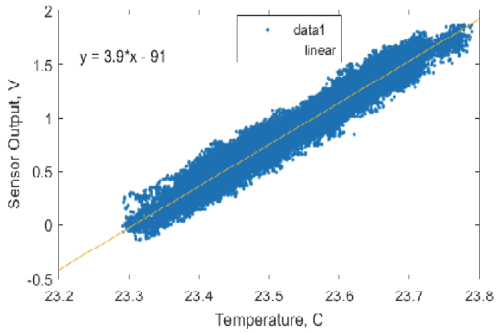


**Fig. 10 Correlation between temperature and sensor output**

A linear dynamic model was extracted using the temperature signal as its input and the sensor signal as the model output. The model was then used to subtract component due to temperature fluctuations. Since experiments were carried at zero net flow, the compensated signal has zero mean as shown by the red trace in Figure 11. Fourier transforms of the raw (original) signal and the compensated one are shown in Figure 12. As evident from the figure, the highest peak in the spectrum appeared near 0.4 mHz, corresponding to a period of about 40 minutes. Most likely this period corresponds to the cycle of the air conditioning system in the lab. Additionally a lower frequency peak near 2.3e-5 Hz (12 hours) is also noticeable. Its magnitude was also attenuated as a

result of the dynamic compensation, resulting in 0.2 V-rms amplitude ( flow rate of 10.5 mL/hr-rms) Over 12-hour period, such drift would constitute a significant volumetric error of about 126 mL, not acceptable for th envisioned application..

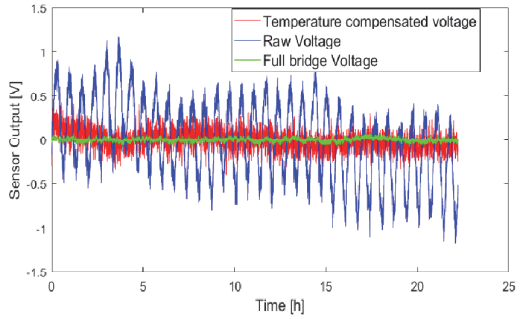


**Fig.11Raw voltage output vs. temperature compensated output vs full sensor bridge output**

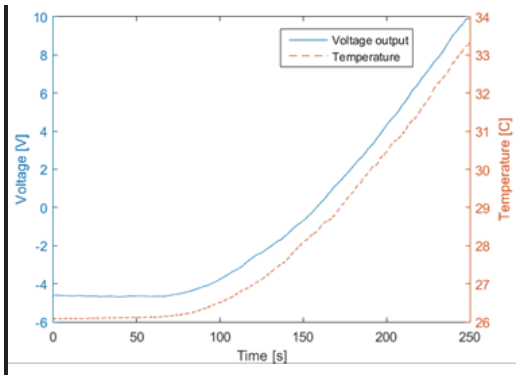


**Fig. 12 FFT of original vs. temperature compensated signal**

Further reduction of the thermal drift requires detailed analysis of each sensor component. These are the three resistors and the magnetic field sensor forming the Wheatstone bridge. Data from the manufacturer indicated that the MTJ sensor has a coefficient of thermal resistance of 0.0006 and a nominal resistance of 1340 Ω. Correspondingly, the anticipated resistance change is 0.8 Ω for every degree Celsius of thermal fluctuation. Assuming that no other component varies with temperature, under the gain of 3300, the output fluctuation is expected to be 2.456 V for each degree of temperature change. The measured thermal sensitivity was however 3.9 V/ ˚C, thus suggesting that other components contribute to the thermal drift. To confirm this, the MTJ sensor was placed in an oven and tested over a range of 26 to 33 ˚C. The raw data and correlation plot of this test are shown in figures 13 and 14 respectively. A thermal sensitivity of 2 V/ ˚C was obtained experimentally while the value estimated from manufacturing data is 2.456 V/ ˚C. The good agreement between the two values suggest that indeed in addition to the MTJ sensor, other components in the circuit contribute to the thermal drift. Most likely these are the through-hole resistors used to complete the bridge. Matching the TCR coefficient of these components is likely to significantly reduce the overall temperature sensitivity and low-frequency drift.

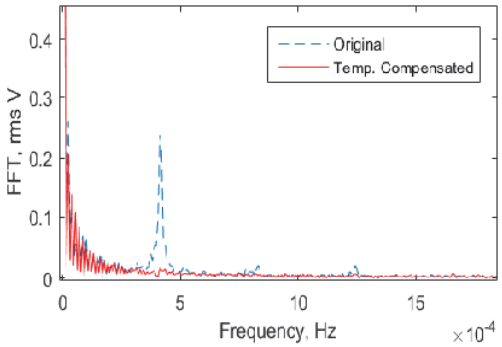


**Fig. 13 Temperature and voltage output of the circuit**

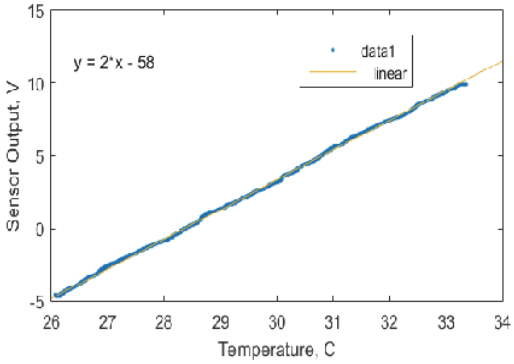


**Fig. 14Correlation between temperature and magnetic sensor output**

## C. Electromagnetic Shielding

Another issue presented in the previous analysis was the presence of the high frequency noise induced by electromagnetic fields. In order to decrease the amount of noise, an electromagnetic Faraday cage was placed around the sensors.

After placing the shield around the sensors the amplitude of the random noise picked up by the sensors has been reduced from 150mV to 50 mV. The comparison between the signals with and without the shield is shown in Figure 15 and Figure 16

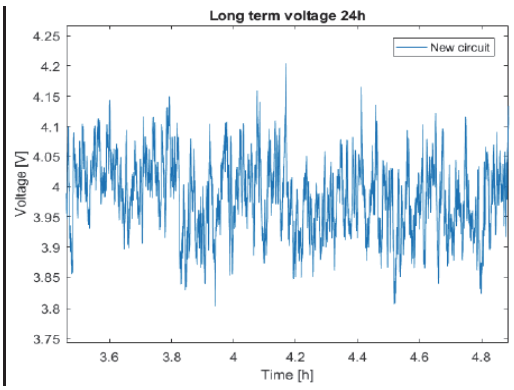


**Fig. 15 Signal noise without electromagnetic shielding**

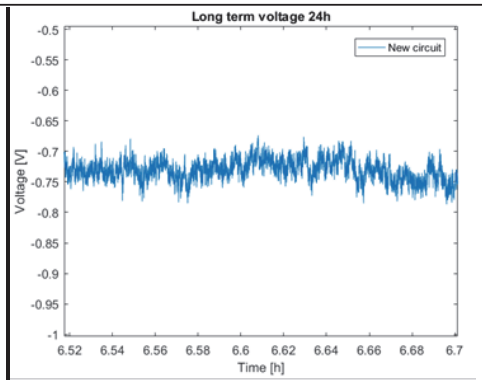


**Fig. 16 Signal noise with electromagnetic shielding**

### D. Full bridge Circuit

One of the greatest challenges faced during the design of this device was the sensor sensitivity required to capture the nominal flow rates of the CSF. One way to improve of the sensitivity is to introduce multiple sensors that work together. To demonstrate the sensitivity gain, we have implemented four MTJ magnetic sensors in a Wheatstone bridge with four nickel transducers underneath the sensors to help us increasing the signal to nose ratio. The orientation of the sensors has been optimized for maximum sensitivity when placed in a bridge configuration. Tests data at various flow rates are shown in Figure: 17. As anticipated, the sensitivity has improved from 25 mV/mL/h to 180 mV/mL/h without increasing the noise level. This corresponds to a 7.2 fold increment in signal to noise ratio. The circuit placement and resistance change directions of the MTJ sensors in the Wheatstone bridge is shown in Fig. 18and the physical placement of the sensors along with their sensitive directions is shown in Fig. 19.

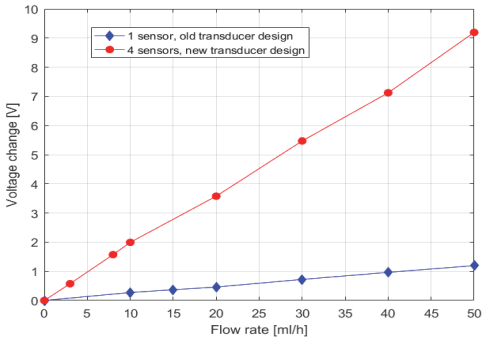


**Fig. 17 Calibratiion curves comparing one sensor vs four sensors**

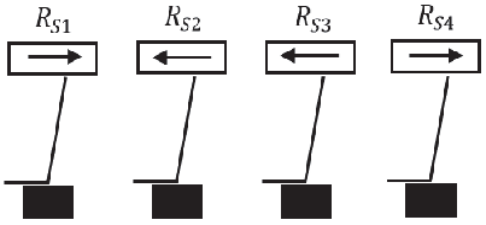


**Fig. 18 MTJ sensors in the Wheatstone bridge**

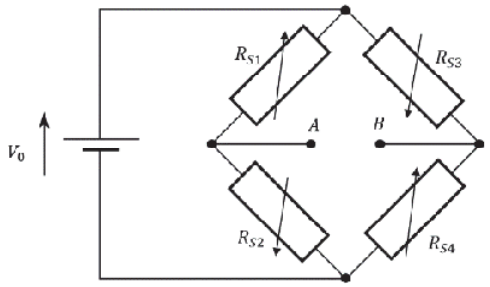


**Fig. 19 Orientation of the MTJ sensors along the flow channel**

In order to quantify the amount of thermal drift over a 24-h period, the signal data was integrated to obtain volume fluctuation over a 24-h period (under net zero flow). Figure 20 shows the results of the integration where we can see that the maximum measurement error during the day is -1.8/+3.2 ml.

Assuming that a typical patient has an average brain pressure-volume compliance of 0.68 ml/mmHg [11], and that they require total CSF diversion due to complete CSF resorption obstruction, the sensitivity to detect intracranial pressure changes of 5 mmHg (corresponding to the accumulation of 3.4ml of additional volume within the CSF space) should be achievable. With an upper limit of normal and cranial pressure (ICP) in adults of 15 mmHg and a lower limit of elevated ICP of 20 mmHg, sensitivity within ± 5 mmHg [10] should allow for measurement and possible intervention prior to any clinically significant elevations in intracranial pressure. Fig.20 shows that our volume measurement error is -1.8/+3.2 ml, which stays below the critical value of 3.4 mL, corresponding to ± 5 mmHg pressure fluctuation. Thus, the proposed sensor has sufficient accuracy for taking flow measurements without clinically significant elevations of ICP.

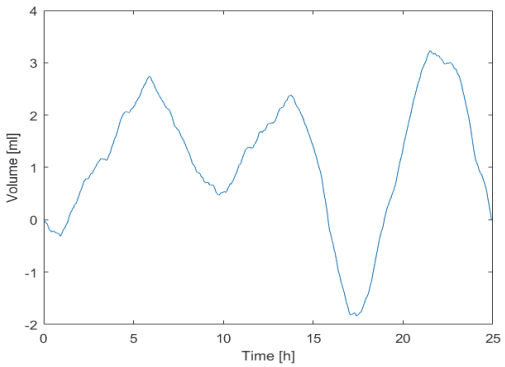


**Fig. 20 Volume error during a 24 h period**

### E. Corrosion Analysis

Another concern of the nickel transducer design is the limited corrosion resistance of nickel and the health concerns about nickel molecules entering the human body. The maximum allowable nickel intake per day for the human body is 200 µg, the weight of one nickel transducer is 5.85 µg which indicates that gradual corrosion of the transducer cannot cause

harm to the patient's health. Another concern regarding corrosion is the risk of the transducer losing enough material thus compromising its functionality. In order to determine the corrosion rate of the nickel transducers a corrosion analysis was performed using cyclic voltammerty. The test was performed using the Gamry PCI4/300 potentiostat and an electrolytic cell. The cell consisted of a graphite counter electrode a nickel working electrode and a Ag/Agcl reference electrode. The solution used in the cell was 1000 ppm $NaSO_4$ with a pH level of 6.85, which is close to the pH level of CSF, thus providing a good representation of an implanted device. The test was performed multiple times with and without a corrosion resistant coating on the nickel. The model we use for the corrosion rate calculations is based on Tafel equation (1)

$$I = I_0 e^{\frac{2.303(E-E_0)}{\beta}}$$

which is expanded for anodic-cathodic reactions resulting in a corrosion model based on Butler-Volmer equation Eq. (2)

$$I = I_{corr}\left(e^{\frac{2.303(E-E_{corr})}{\beta_a}} - e^{\frac{-2.303(E-E_{corr})}{\beta_c}}\right)$$

whereI is the measured current from the cell, $I_{corr}$is the corrosion current, E is the electrode potential, $E_{corr}$ is the corrosion potential and $\beta_a$ and $\beta_c$ are the anodic and cathodic Tafel constants.The resulting I-V curve in logarithmic scale is shown in Fig.21. The corrosion current is than obtained by extrapolating the linear portions of the logarithmic curves in Fig.21 and determining the current at their intersection point for the anodic and cathodic regime and taking the average of the two. The corrosion rate is then calculated from Eq. (3), where $I_{corr}$ is the corrosion current, K defines the units for the corrosion rate (in our case $K = 3272$ A-cm-year), $W_e$ is the equivalent weight d is the density and A is the sample area.

$$C_R = \frac{I_{corr} \cdot K \cdot W_e}{d \cdot A}$$

The tabulated results for the measured corrosion rates can be seen in Table 1 below and the raw output of the cyclic voltammetyis in Figure 21. Data from the table indicate a lifespan of 15 to 55 years for a 10-µm--thick transducer element.

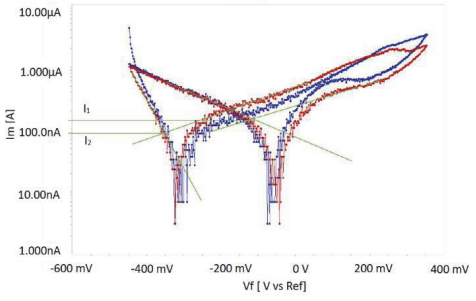


**Fig. 21 Corrosion analysis output**

**Tab. 1 Corrosion analysis results**

| | $I_{corr}$ | $C_r$ |
|---|---|---|
| Test1 (uncoated) | 22 nA | 0.24 µm/year |
| Test 2 (uncoated) | 30 nA | 0.32 µm/year |
| Test 3 (coated) | 12 nA | 0.13 µm/year |
| Test 4 (coated) | 9 nA | 0.09 µm/year |

### F. Dynamic Flow Testing

Given the anticipated pulsatile nature of the CSF flow, the sensor will likely be exposed to variable flows with frequency near that of the heart. Therefore analysis of its performance under variable flow conditions was undertaken. The test apparatus included a peristaltic pump with four rollers producing pulsatile flow. Recording from the sensor measuring such flow are shown in Figure 22. The pump was driven in forward (first half of the plot) and reverse (second half of the plot) direction. Fitting exponential (first-order) response to the portion when the pump was stopped showed a transient with a time-constant of 0.4 seconds. Therefore, the sensor's response time is near or below this value.

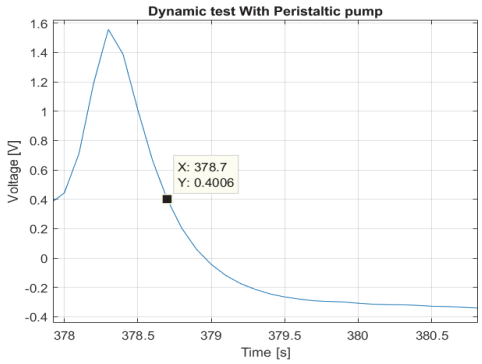


**Fig. 22. Signal output during dynamic testing**

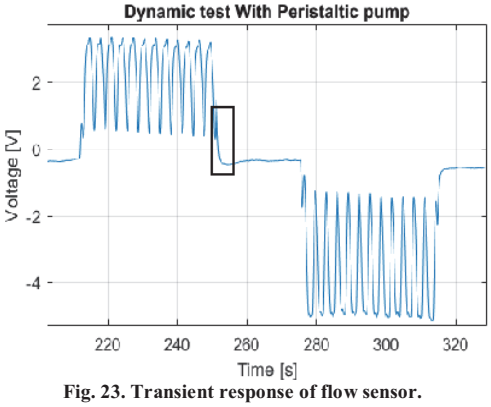


**Fig. 23. Transient response of flow sensor.**

## DISCUSSION AND CONCLUSIONS

Optimization of the geometry of previously-designed flow sensor demonstrated increased sensitivity and

signal to noise ratio. Low frequency drift was shown to be due to thermal fluctuations impacting the resistors in the bridge and the operational amplifiers. When four MTJ sensors with matched TCR coefficients are used in the Wheatstone bridge the temperature induced signal drift is reduced to -1.8/+3.2 mL per 24-hour period.

The present study showed that it is possible to increase the sensitivity of the previously proposed flow sensor by changing the architecture of the ferromagnetic transducer. It was also shown that the suspected thermal sensitivity of the sensor is present in both the transducer element as well as in the amplification circuit.

Through careful resistor selection in the Wheatstone bridge, or with the use of four MTJ magnetic sensors with equal TCR values connected in the Wheatstone bridge, it is possible to reduce the low frequency temperature related signal drift down -1.8/+3.2 mL per 24-hour period. These values are below the allowable volume change for the ventricles of an adult brain.

The sensitivity of the sensor device has also been improved by the introduction of a full-bridge sensing circuit with four magnetic transducers, increasing the sensitivity 7.2 fold.

Through the introduction of electromagnetic shielding an improvement in the signal to noise ratio by a factor of 5 was achieved. A corrosion analysis has been performed indicating a possible 15 to 55 years of life span of the device. The dynamic response of the sensor appears adequate for the intended application.

## REFERENCES


[1] Y. Wu, N. L. Green, M. R. Wrensch, S. Zhao, N. Gupta, Ventriculoperitoneal shunt complications in california: 1990 to 2000, Neurosurgery 61 (3) (2007) 557-563.

[2] H. J. Garton, J. R. Kestle, J. M. Drake, Predicting shunt failure on thebasis of clinical symptoms and signs in children, Journal of neurosurgery 94 (2) (2001) 202-210.

[3] J. M. Drake, J. R. Kestle, R. Milner, G. Cinalli, F. Boop, J. Piatt Jr,S. Haines, S. J. Schi, D. D. Cochrane, P. Steinbok, et al., Randomized trial of cerebrospinal fluid shunt valve design in pediatric hydrocephalus, Neurosurgery 43 (2) (1998) 294-303.

[4] J. Kestle, J. Drake, R. Milner, C. Sainte-Rose, G. Cinalli, F. Boop, J. Piatt, S. Haines, S. Schi, D. Cochrane, et al., Long-term follow-up data from theshunt design trial, Pediatric neurosurgery 33 (5) (2001) 230-236.

[5] L. Acakpo-Satchivi, C. N. Shannon, R. S. Tubbs, J. C. Wellons III, J. P.Blount, B. J. Iskandar, W. J. Oakes, Death in shunted hydrocephalic children: a follow-up study, Child's Nervous System 24 (2) (2008) 197-201.

[6] R. V. Patwardhan, A. Nanda, Implanted ventricular shunts in the UnitedStates: the billion-dollar-a-year cost of hydrocephalus treatment, Neurosurgery 56 (1) (2005) 139-145.

[7] J. R. Atkinson, D. B. Shurtle, E. L. Foltz, Radio telemetry for the measurement of intracranial pressure., Journal of neurosurgery 27 (5) (1967)428.

[8] V. Macellari, Batteryless on-demand-sampling active radiosonde for intracranial pressure measurement, Medical and Biological Engineering and Computing 19 (6) (1981) 686-694.

[9] E. T. Enikov, G. Edes, J. Skoch, R. Anton, Application of gmr sensors to liquid flow sensing, Journal of Microelectromechanical Systems 24 (4) (2015) 914-921.

[10] J. Miller, J. Garibi, Intracranial volume/pressure relationships during continuous monitoring of ventricular fluid pressure, in: Intracranial pressure, Springer, 1972, pp. 270-274.

[11] G. Portella, M. Cormio, G. Citerio, C. Contant, K. Kiening, P. Enblad,I. Piper, Continuous cerebral compliance monitoring in severe head injury:its relationship with intracranial pressure and cerebral perfusion pressure,Actaneurochirurgica 147 (7) (2005) 707-713.


★★★